Quantum Efficiency of a Back-illuminated CCD Imager: An Optical Approach

D. E. Groom,[a] S. E. Holland,[a] M. E. Levi,[a] N. P. Palaio,[a] S. Perlmutter,[a]
R. J. Stover,[b] and M. Wei[b]

[a]Lawrence Berkeley National Laboratory, Berkeley, CA 94720

[b]University of California Observatories/Lick Observatory,
University of California at Santa Cruz, Santa Cruz, CA 95064

ABSTRACT

We have developed an optical approach for modeling the quantum efficiency (QE) of back-illuminated CCD optical imagers for astronomy. Beyond its simplicity, it has the advantage of providing a complete fringing description for a real (wide-aperture) system. Standard thin-film calculations are extended by (a) considering the CCD itself as a thin film, and (b) treating the refractive index as complex. The QE is approximated as the fraction of the light neither transmitted nor reflected, which basically says that all absorbed photons produce e-h pairs and each photoproduced e or h is collected (recombination is negligible). Near-surface effects relevant to blue response must still be treated by standard semiconductor modeling methods. A simple analytic expression describes the QE of a CCD without antireflective (AR) coatings. With AR coatings the system is more easily described by transfer matrix methods. A two-layer AR coating is tuned to give a reasonable description of standard thinned CCD's, while the measured QE of prototype LBNL totally-depleted thick CCD's is well described with no adjustable parameters. Application to the new LBNL CCD's indicates that these devices will have QE $> 70\%$ at $\lambda = 1000$ nm and negligible fringing in optical systems faster than $\sim f4.0$.

Keywords: CCD, high resistivity, fully depleted, astronomical, Lick Observatory, Lawrence Berkeley National Laboratory

1. INTRODUCTION

In the extended optical region (320 nm $\lesssim \lambda \lesssim$ 1000 nm), the optical absorption length in silicon changes by over four orders of magnitude, from $\ell \approx 9$ nm at $\lambda = 350$ nm to about 135 μm at 1000 nm[1,2,5] (Figure 1(a)). This circumstance is of exigent importance in trying to optimize both blue and red response. At the blue end of the spectrum an assortment of near-surface problems must be solved.[6–8] For increasingly red light the device gradually becomes transparent, resulting in reduced quantum efficiency (QE) and fringing due to the interference of multiple reflections. Typical fringing behavior in a thinned, back-illuminated CCD is shown in Figure 2.

We restrict our attention to back-illuminated devices in which the substrate is completely active, either through thinning or by using a high-resistivity substrate. In the latter case the substrate may or may not be totally depleted, although depletion is necessary to minimize the effects of lateral diffusion.[9] Except at the blue end of the spectrum, photons produce e-h pairs far enough from the back surface and with a sufficiently long lifetimes that all of the charge is collected by the CCD.[10] In this case we can equate the fractional intensity absorbed at a given wavelength with quantum efficiency, and the problem can be treated in completely optical terms.

To do this, we must consider the *amplitude* of the incident wave, not its intensity. Adding intensities might give a good result for the average QE,[6,7] but will not give fringing information. We use standard optical methods with two departures: The CCD is itself treated as a "thin film," along with any antireflection (AR) coatings, and the index of refraction is allowed to be complex, so that light can be absorbed.

Since the LBNL CCD's are made on an n-type substrate that is biased with a positive voltage, the usual problems associated with an e^- accumulation under the back intrinsic oxide layer are avoided. On the other hand, a P-doped polysilicon layer is necessary to form the ohmic contact on the wafer back side. This layer is absorptive in the blue,[11] with the result that these CCD's have about the same blue response as normal thinned CCD's. We have attempted to

Author information for DEG: deg@lbl.gov, http://pdg.lbl.gov/~deg/ccd.html

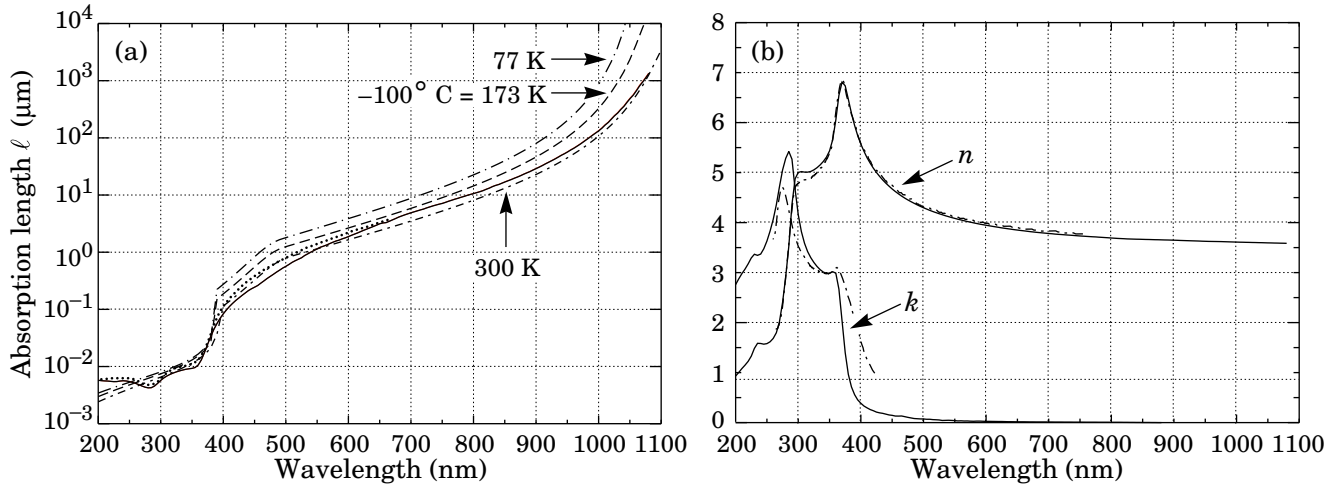

Figure 1. (a) Absorption length of light ℓ in silicon. The room-temperature (300 K) solid curve is from Refs. 1 and 2. The dashed curves are calculated from the phenomenological fits by Rajkanan *et al.*[3] (b) Real and imaginary parts of the index of refraction of silicon ($n_c = n + ik$, and $k = \lambda/4\pi\ell$). Our best values for these data, indicated by the solid curves, are available in the form of an interpolated text table at `http://pdg.lbl.gov/~deg/ccd.html`.

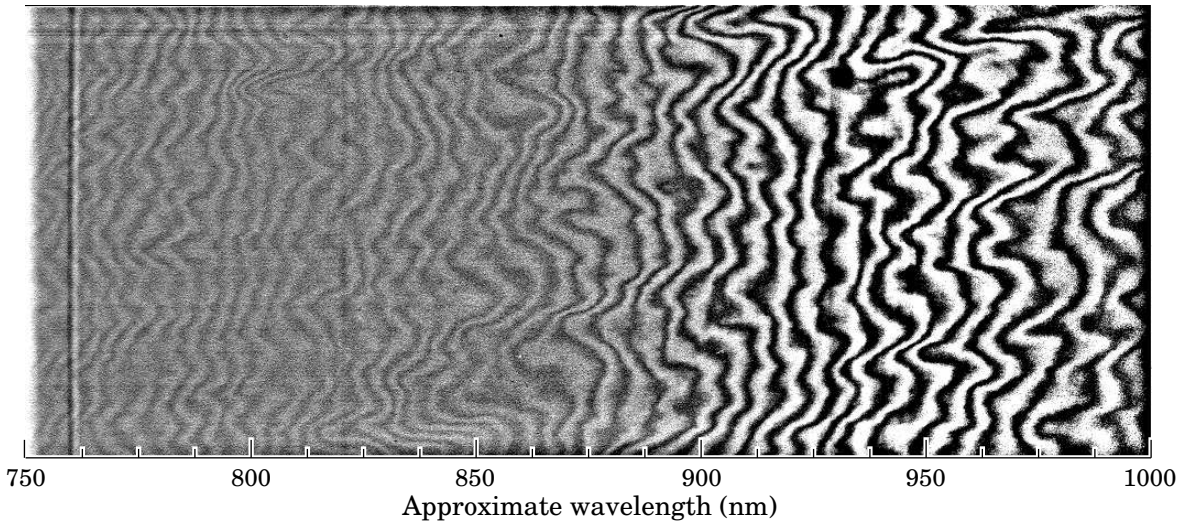

Figure 2. A white-light exposure with the Keck low-resolution spectrograph (LRIS),[4] divided by the same frame averaged over 50 adjacent pixels. The image is 1000 pixels long (in the dispersion direction) and 500 wide (along the slit). This image enhances the fringes, which are at the 1% level at 800 nm and 5% level at 950 nm. The fringe spacing should be $\delta\lambda = \lambda^2/2nd$, where the thickness is d and the index of refraction is $n \approx 3.65$. There are about 8 fringes between 900 and 950 nm, from which one concludes that the CCD is 20–22 μm thick. The spectrum was supplied by I. M. Hook, who obtained the image in 1994 November.

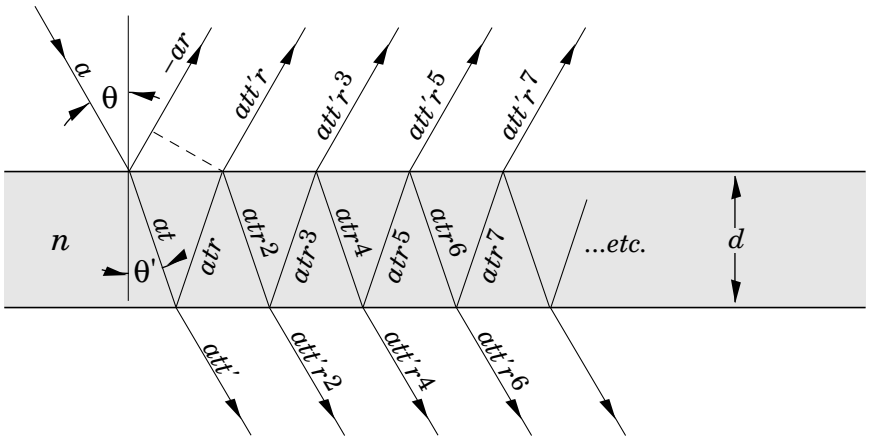

Figure 3. Amplitudes of successive rays in multiple reflections from a chip with index n and thickness d. Successive reflections are retarded by a phase ϕ, where $\phi = 4\pi nd\cos\theta'/\lambda$, and attenuated by a factor $\exp(-d/\ell\cos\theta')$ on each transit.

model the behavior by assuming that any charge produced in this region is lost. Experimental measurements indicate higher blue response than this "hard kill" model predicts, very likely because diffusion out of the layer competes with recombination. Pending more realistic modeling by solid-state methods, we roughly indicate the expected behavior by a dashed line blueward of about 400 nm in the QE figures in this paper.

2. OPTICAL CONSTANTS FOR SILICON

The complex index of refraction is

$$n_c = n + ik\ , \tag{1}$$

where $k = \lambda/4\pi\ell$ and ℓ is the absorption length. (We have chosen to express the absorption in terms of the absorption length, ℓ, because of its more intuitive connection to physical thicknesses in the problem.) The reflectivity for light normally incident on an air (or vacuum) boundary is

$$R = \frac{(n-1)^2 + k^2}{(n+1)^2 + k^2}\ . \tag{2}$$

Optical constants for silicon at room temperature (300 K) for $\lambda < 750$ nm have been taken primarily from the *Handbook of Optical Constants for Solids*[1,12]; see also Jellison and Modine.[5] Extension to longer wavelengths has been made via the reflection and absorption curves from Ref. 2. In general the red data are more dependable, since low reflectivity can more easily be measured than high ($R \approx 33\%$ at 800 nm), and absorption can be measured using thick samples and without serious reflectivity correction errors.

The absorption length is shown in Fig. 1(a). The data below 750 nm from Ref. 2 are shown by the dotted curve. CCD response near the bandgap cutoff is particularly temperature dependent due to the physics of absorption via indirect transitions requiring phonons.[13–15] We have used the phenomenological fits by Rajkanan *et al.*[3] to calculate the absorption lengths at 77, 173, and 300 K, shown by the dashed curves in Fig. 1(a). For $\lambda > 800$ nm the 300 K absorption length is $\lesssim 30\%$ lower than that given by Janesick,[2] perhaps reflecting the older data fitted by Rajkanan *et al.* The increased absorption length at $-100°$ C is equivalent to a shift to the blue by 55 nm at $\lambda = 1000$ nm. The sharp drop of QE at about this wavelength will be similarly displaced to shorter wavelengths.

The real and imaginary parts of n_c are shown in Fig. 1(b). Some measure of the differences in published data is provided by the dashed curves for n and k, taken from Jellison and Modine.[5] It is clear from Eq. 2 and Fig. 1(b) that the complex part of the refractive index is of little importance for most purposes for $\lambda > 400$ nm. The exception is for the phase shift in a thick film, where the imaginary part produces absorption, and, incidentally, quantum efficiency.

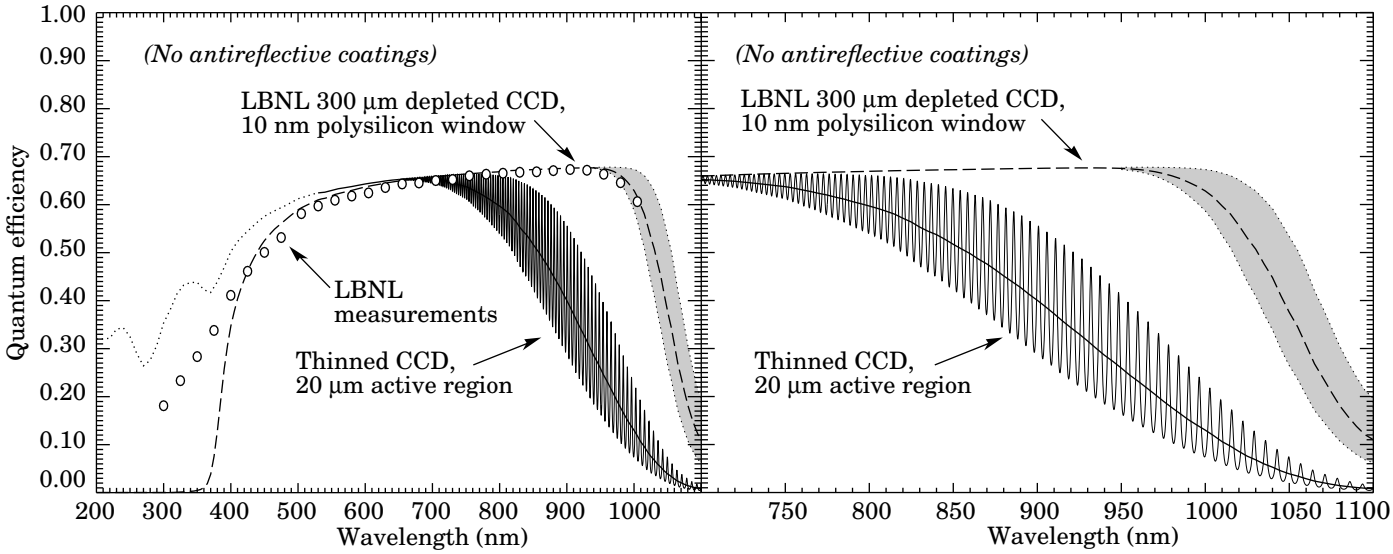

Figure 4. Quantum efficiency as calculated using Eq. 6, for a thinned CCD with a 20 μm active region and for the LBNL CCD using a totally depleted high-resistivity silicon wafer 300 μm thick. In the latter case, a 10-nm polysilicon coating on the back window, needed for gettering and electrical contact purposes, was modeled by "killing" all charge photoproduced in the layer. As can be seen by the comparison with experiment, the response in the blue is actually better. In the thinned CCD case the blue end (dashed) is not modeled, but practical devices seem to have about our measured QE in this region. The fringe spacing is in agreement with that shown in Fig. 2.

3. NO ANTIREFLECTIVE COATING CASE

Considerable insight is gained by an elementary analysis for the case of a CCD without an antireflective coating. We consider a plane wave of light (vacuum wavelength λ, electric field amplitude a) incident at an angle θ to the normal on a silicon "film" with thickness d. The geometry is shown in Figure 3. The refracted ray makes an angle θ' to the normal. After each successive reflection or transmission the phase is retarded by a phase $\phi = 4\pi nd\cos\theta'/\lambda$ from the previous one. The amplitude is attenuated by a factor $\exp(-d/\ell\cos\theta')$ on each transit, where ℓ is the *intensity* attenuation length.* (The $\cos\theta'$ term is in the numerator of the phase shift expression because of the phase delay of the previous directly reflected ray; see Ref. 16 or other optics text for a derivation.)

A fraction r of the amplitude survives a single reflection, with a phase reversal if the light is going from air to silicon. A fraction t is transmitted in going from air to silicon, and t' from silicon to air. Following the notation of Figure 3, we may write the reflected amplitude a_R as

$$\begin{aligned} a_R/a &= -r + tt're^{i\phi}e^{-d/\ell'}(1 + r^2e^{i\phi}e^{-d/\ell'} + r^4e^{2i\phi}e^{-2d/\ell'} + r^6e^{3i\phi}e^{-3d/\ell'} + \ldots) \\ &= -r + \frac{tt're^{i\phi}e^{-d/\ell'}}{1 - r^2e^{i\phi}e^{-d/\ell'}} \\ &= -r\left[\frac{1 - e^{i\phi}e^{-d/\ell'}}{1 - r^2e^{i\phi}e^{-d/\ell'}}\right] , \end{aligned} \tag{3}$$

where $\ell' = \ell\cos\theta'$. For the last step, we used Stokes' time-reversal argument[17] that $tt' = (1 - r^2)$. It is the use of this equality which makes it difficult to include the effects of an antireflective coating in this method.

The absolute value squared of the expression in Fig. (3) gives the fractional reflected intensity:

$$\frac{I_R}{I_0} = r^2\frac{1 - 2e^{-d/\ell'}\cos\phi + e^{-2d/\ell'}}{1 - 2r^2e^{-d/\ell'}\cos\phi + r^4e^{-2d/\ell'}} \tag{4}$$

*Alternatively, $\phi = (4\pi d/\lambda)(n\cos\theta' + ik/\cos\theta')$, and the $e^{i\phi}$ term includes the attenuation. Compare with Eq. (1).

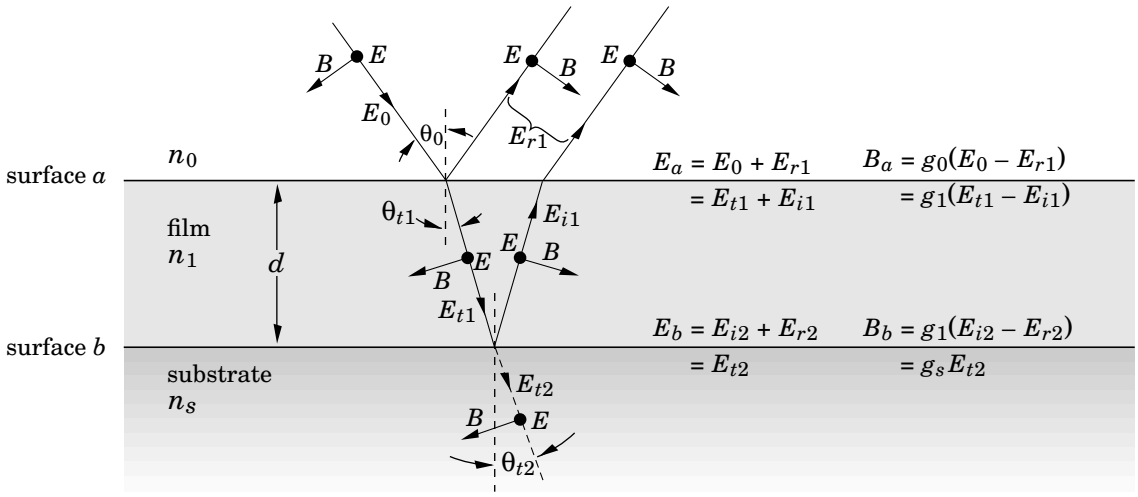

Figure 5. Reflection of a beam from a single film for the case of E field (bold dot) parallel to the surface and perpendicular to the plane of incidence. The arrows perpendicular to the ray indicate the direction of B. The incident electric field magnitude is E_0, the net reflected magnitude from surface a is E_{r1}, and the transmitted magnitude (into the substrate) is E_{t2}. The EM boundary conditions relate (E_a, B_a) and (E_b, B_b) via the transfer matrix for the film, and the decomposition into incident, reflected and transmitted fields on either side of the surfaces as given in the figure permits solution for E_{r1} and E_{t2}. Independently of incident wave polarization, $g_{0c} = n_0 \cos\theta_0$ and $g_s = n_{sc} \cos\theta_{t2}$ for $\sqrt{\epsilon_0 \mu_0} \equiv 1$.

By a parallel argument, the fraction of the light which is transmitted is given by

$$\frac{I_T}{I_0} = \frac{(1-r^2)^2 e^{-d/\ell'}}{1 - 2r^2 e^{-d/\ell'} \cos\phi + r^4 e^{-2d/\ell'}} \ . \tag{5}$$

To our approximation that every absorbed photon results in a collected e or h, the quantum efficiency is given by the fraction of the intensity not reflected or transmitted, i.e. absorbed:

$$QE = 1 - I_R/I_0 - I_T/I_0 = \frac{(1-r^2)[1 - (1-r^2)e^{-d/\ell'} - r^2 e^{-2d/\ell'}]}{1 - 2r^2 e^{-d/\ell'} \cos\phi + r^4 e^{-2d/\ell'}} \tag{6}$$

The transmitted and reflected intensity profiles are the same as those for a Fabry-Perot interferometer except for the exponential terms. Equation (6) may also be compared to Eq. (8) in Ref. 7. The main difference is the $\cos\phi$ factor in the denominator, which carries the fringing information.

Quantum efficiencies calculated via Eq. (6) for a thinned CCD with a 20 μm active region and for the 300-μm thick LBNL high-resistivity CCD are shown in Fig. 4. In the expanded view in the right panel of the figure it can be seen that the fringe profile is not sinusoidal, but has the characteristic Haidinger fringe shape. The upper and lower envelopes can be calculated using $\cos\phi = \pm 1$, but the average QE is slightly lower than their average because of the asymmetric fringe profile.

Since the 300-μm thick CCD exhibits fringes which are are 15 times closer together than for a thinned CCD, they are shown as a grey band in Fig. 4. This calculation is for normally incident light ($\cos\theta = \cos\theta' = 1$). In a typical instrument there is a range of incidence angles, and as a result close fringes tend to get washed out. This issue will be explored in Sect. 6.

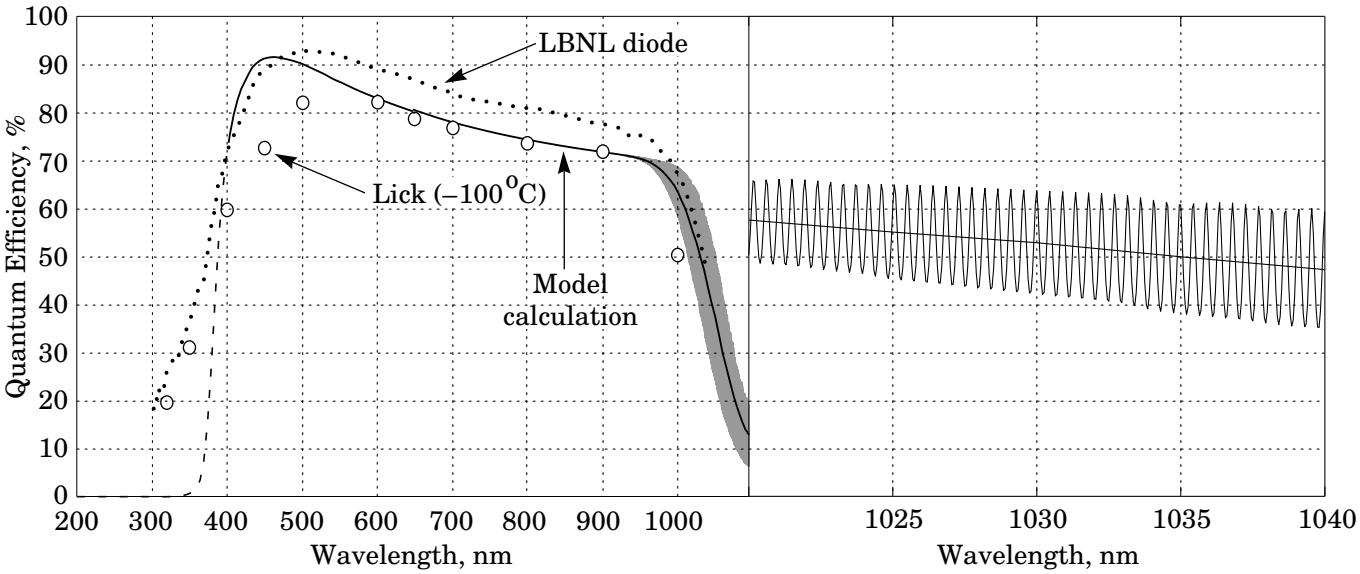

Figure 6. Quantum efficiency for the LBNL prototype back-illuminated CCD's.[8,18,19] The back surface was coated with 10 nm of polysilicon and 50 nm of ITO ($n \approx 2$ at $\lambda = 440$ nm), which served both as a back electrode and as an AR coating optimized for the blue. The solid curve plus the grey oscillating section in the left panel show the QE calculation using the transfer matrix method, using absorption data for 300° K. Diffusion of charge out of the back polysilicon layer was ignored, leading to the conservative (dashed) result for $\lambda < 400$ nm. The solid curve through the fringe region is the average of the upper and lower envelopes. The Lick measurements (white circles) are for a cold CCD, while the LBNL measurements (dotted curve) were obtained with a room-temperature "identical" photodiode. The right panel shows an expansion of a 20 nm interval in the fringe region.

4. TRANSFER MATRIX APPROACH

A summation over the many orders of reflection or transmission shown in Fig. 3 becomes essentially impossible if there is more than one layer. It is much easier to solve the electromagnetic (EM) boundary value problem for a single layer, and then combine the N results if there are N layers.† The geometry and variables are shown in Fig. 5. In this approach, the reflected beam consists of the directly reflected wave plus the sum of the multiple waves reflected from the back surface of the "film." Similarly, the wave transmitted into the substrate includes all multiple reflections in the film. The case shown is for an electric field parallel to the surface.

Invoking the boundary conditions at surfaces a and b, one finds

$$\begin{pmatrix} E_a \\ \\ B_a \end{pmatrix} = \begin{pmatrix} \cos\delta & \dfrac{i\sin\delta}{g_1} \\ \\ ig_1\sin\delta & \cos\delta \end{pmatrix} \begin{pmatrix} E_b \\ \\ B_b \end{pmatrix} \equiv \mathcal{M} \begin{pmatrix} E_b \\ \\ B_b \end{pmatrix} \tag{7}$$

Here $g_1 = n_{1c}\cos\theta_{t1}$,‡ and we have set $\sqrt{\epsilon_0\mu_0} = 1$ (it eventually cancels anyway). The phase shift δ is half of the phase shift ϕ defined in the previous section, except that in the case of an absorptive medium (the CCD) we include a complex part:

$$\begin{aligned} \delta &= 2\pi d n_1 \cos\theta_{t1}/\lambda - id/2\ell\cos\theta_{t1} \\ &= (2\pi d/\lambda)(n_1\cos\theta_{t1} + ik/\cos\theta_{t1}) \end{aligned} \tag{8}$$

†This discussion and notation are based on Pedrotti & Pedrotti (Ref. 16). The main departures are the introduction of complex phase and refractive index.

‡For the opposite polarization (B parallel to the surface), $g_1 = n_{1c}/\cos\theta_{t1}$ while g_0 and g_s (defined in the figure caption) remain the same.

The 2×2 transfer matrix for the film,

$$\mathcal{M} = \begin{pmatrix} m_{11} & m_{12} \\ m_{11} & m_{12} \end{pmatrix} , \tag{9}$$

depends only on the properties of the film in question. If there are N films, then

$$\begin{pmatrix} E_a \\ B_a \end{pmatrix} = \mathcal{M}_1 \mathcal{M}_2 \cdots \mathcal{M}_N \begin{pmatrix} E_N \\ B_N \end{pmatrix} \equiv \mathcal{M} \begin{pmatrix} E_N \\ B_N \end{pmatrix} . \tag{10}$$

The final step is to use the expressions for E_a and E_b given in the figure to solve for the amplitudes of the reflected and transmitted waves:

$$r \equiv \frac{E_{r1}}{E_0} = \frac{g_0\, m_{11} + g_0 g_s\, m_{12} - m_{21} - g_s\, m_{22}}{g_0\, m_{11} + g_0 g_s\, m_{12} + m_{21} + g_s\, m_{22}} \tag{11}$$

$$t \equiv \frac{E_{t2}}{E_0} = \frac{2 g_0}{g_0\, m_{11} + g_0 g_s\, m_{12} + m_{21} + g_s\, m_{22}} \tag{12}$$

(*Note that the symbols r and t are used differently than in the previous section.*) As before, the quantum efficiency of the device is

$$\mathrm{QE} = 1 - |r|^2 - |t|^2 \tag{13}$$

For an uncoated CCD Eq. (13) is algebraically identical to Eq. (6), although the demonstration is fairly tedious.

In spite of the complexity of this development, the formalism is surprisingly easy to apply: One finds the transfer matrix for each layer, including the CCD itself, forms the product, and calculates r and t.

5. RESULTS FOR NORMAL INCIDENCE

For purposes of this paper, we restrict the discussion to three examples: The LBNL prototype thick CCD (for which experimental measurements are available, a conventional thinned CCD, and the LBNL thick CCD which is currently being tested.

The 300-μm thick LBNL CCD requires a bias of 25–35 V for total depletion. The back electrode consists of an indium-tin oxide (ITO) window. This window is transparent in the optical. With an index of refraction of 2.0 at 440 nm, it is a good AR coating for silicon. A sputtered SiO_2 film, with thicknesses tuned for the desired red response optimization, is added to the ITO coating.

The small prototype CCD described in Refs. 8, 18, and 19 had only an ITO coating, with its thickness (50 nm) chosen to optimize blue response. As a result, red response was somewhat compromised. A model calculation and two sets of QE measurements for this CCD are shown in Fig. 6. The grey band is actually fringing, and shows the characteristic Haidinger fringe profile upon scale expansion (right panel). The LBNL measurements were made on a room-temperature "equivalent" photodiode using a monochromator as the light source. The Lick measurements were made with 10-nm bandpass filters on a cold CCD. Some conclusions can be drawn:

1. The low Lick measurement at 1000 nm is probably real, and is consistent with the expected bandgap increase in cooling to -120° C.
2. The model and Lick measurements for 600–900 nm are in good agreement.
3. The Lick and LBNL measurements are in good agreement for $\lambda = 400$ nm and below, and the measured QE in this region is very similar to that obtained with thinned CCD's. The "hard kill" approximation to the polysilicon absorption in this region (dashed line) is far too conservative.
4. The difference between the model calculation and the Lick measurements at 450 and 500 nm is not understood, given that the agreement at longer wavelengths lends credence to the measurements.

For our present purposes, and without knowing the details of any specific AR coating, the thinned CCD was modeled by tuning our ITO and sputtered SiO_2 coatings for a rough match to a published response.[20] The results for parallel incident light are shown in the left panels of Fig. 7. The main difference with previous results is the fringe detail.

The designed response to parallel light for the present LBNL fabrication run is shown in the left panels of Fig. 8, where the black band at $\lambda > 1000$ nm consists of unresolved fringe oscillations.

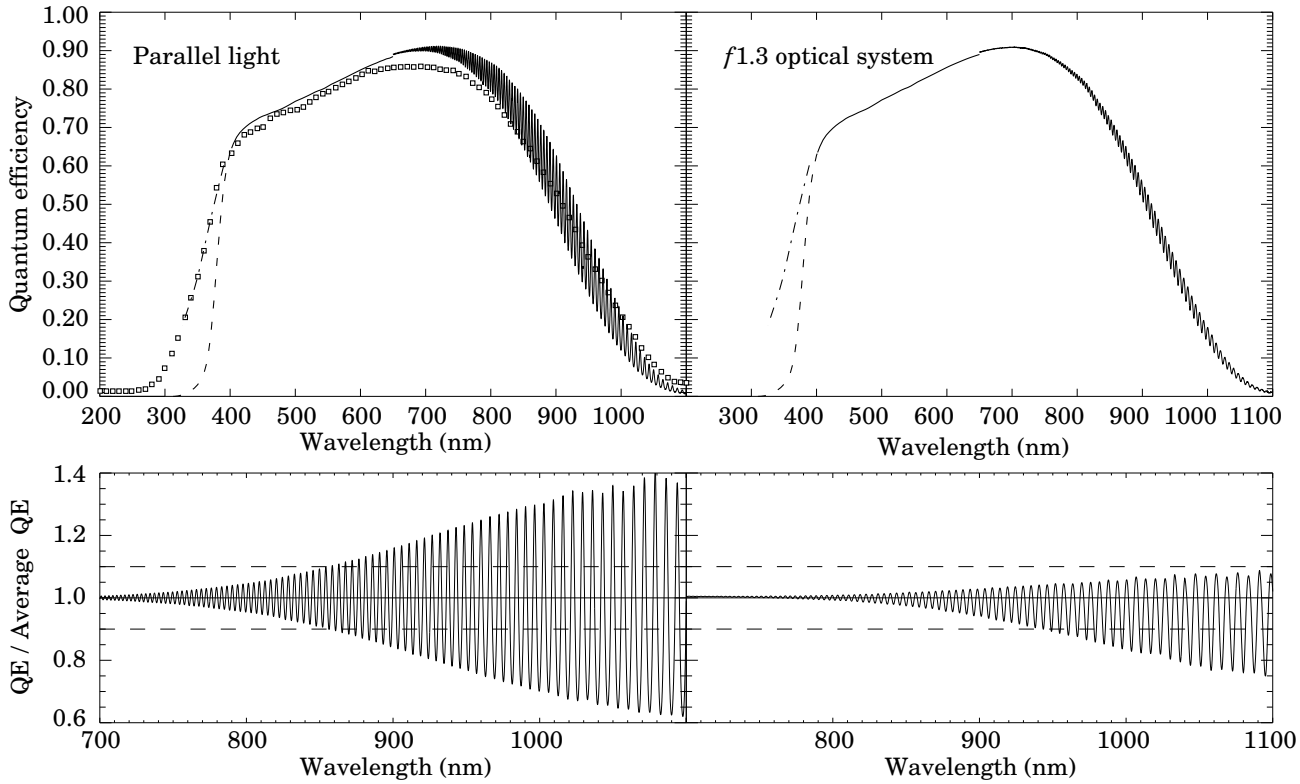

Figure 7. Quantum efficiency and fractional fringe amplitude for a thinned CCD with a 20 μm thick active region. The QE of a typical thinned CCD is shown by the open squares in the top left panel.[20] Diffusion of charge out of the back polysilicon layer was ignored, leading to the conservative (dashed) result for $\lambda < 400$ nm; estimated response is indicated by the dot-dashed curve. The left side shows the expected results for parallel illumination, and the right for an $f1.3$ system.

6. INTEGRATION OVER APERTURE

Equation (13) gives $\mathrm{QE}(\lambda, \theta_0)$, which may be integrated over solid angle to include aperture effects, such as differences of AR coating behavior with angle and the "washout" of fringes due to the change of $d(\mathrm{QE})/d\lambda$ with angle:

$$\langle \mathrm{QE}(\lambda) \rangle = \int_\Omega \mathrm{QE}(\lambda, \theta_0) d\omega \Big/ \int_\Omega d\omega \tag{14}$$

Note that we are averaging the intensity, not the amplitude. Waves arriving at different angles are orthogonal, and do not interfere.

Polarization is treated in a somewhat strange way. If $\mathrm{QE}(\lambda, \theta_0)$ is calculated for an incident wave with its electric vector parallel to the interface, then we are considering polarization which rotates with azimuthal angle. This should be averaged with a results of a calculation with the magnetic vector parallel to the surface ($g_1 = n_c / \cos\theta_{t1}$ instead of $g_1 = n_c \cos\theta_{t1}$). But even for an $f1.3$ system (the Keck LRIS[4]) the minimum value of $\cos\theta_{t1}$ is 0.996 (for $n_{\mathrm{Si}} = 4.0$), so polarization considerations are hardly of consequence.

For purposes of illustration we have chosen a Simpson's integration over an unobstructed circular aperture. The results for our thin CCD model are shown in the right panels of Fig. 7. The mean fractional fringe amplitude drops below unity because we have taken the upper and lower envelope mean as our average. As the wavelength increases this average is increasingly higher than the actual mean because of the Haidinger fringe asymmetry. The results are in qualitative agreement with Fig. 2. More detailed modeling of this system with the CCD in current use is being done by Patrik Jonsson and the UCO/Lick Observatory group.[21]

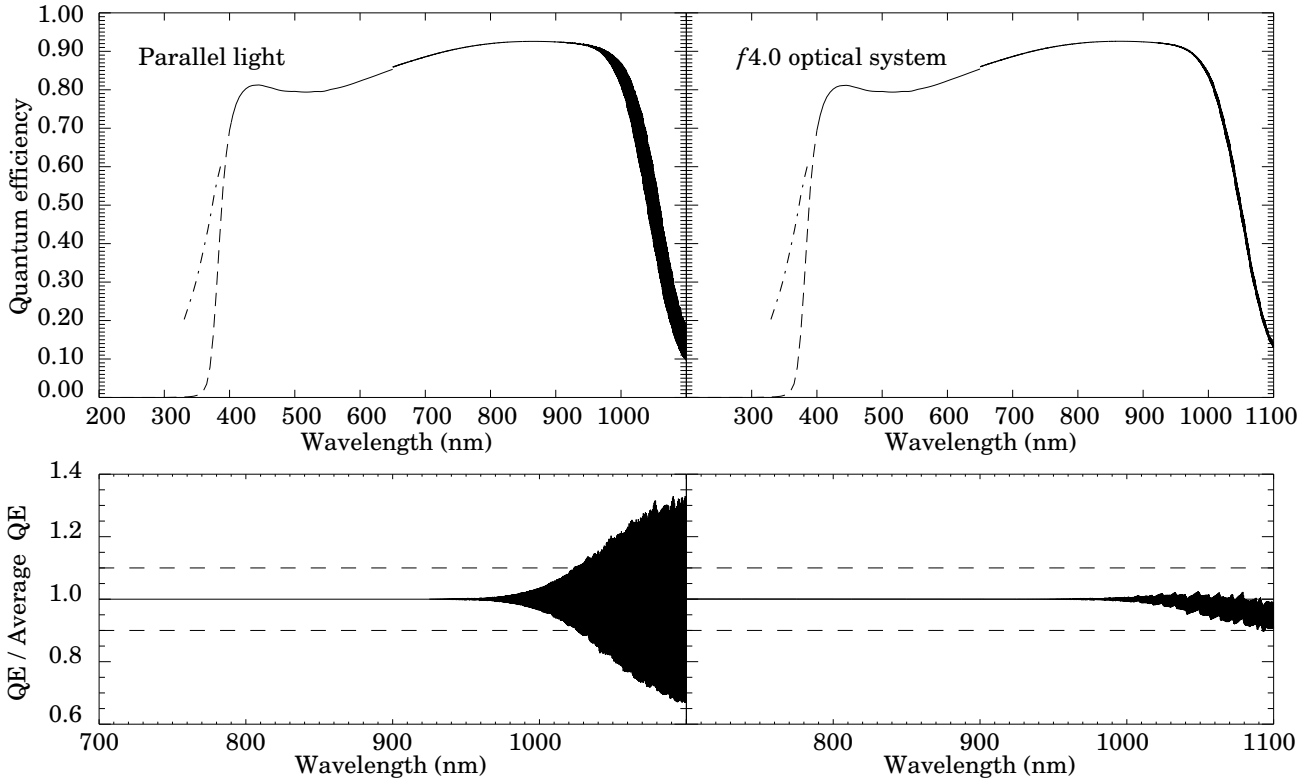

Figure 8. Quantum efficiency and fractional fringe amplitude expected for the LBNL CCD's currently being tested. Diffusion of charge out of the back polysilicon layer was ignored, leading to the conservative (dashed) result for $\lambda < 400$ nm; estimated response is indicated by the dot-dashed curve. The left side shows the expected results for parallel illumination, and the right for an $f4.0$ system.

7. DISCUSSION

This work is incomplete in many ways. All of the QE calculations should be repeated with the best available optical constants, and the red response should be studied as a function of temperature. Additional AR coatings should be added, both theoretically and in the laboratory, to improved the response near 1000 nm where the ITO-SiO_2 combination becomes ineffectual. Solid-state techniques should be used to model behavior for $\lambda < 400$ nm in the case of the LBNL CCD, where diffusion of charge out of the back polysilicon layer is important. Finally, experimental QE measurements of the LBNL CCD, part of the present characterization effort, should be added to Fig. 8 as soon as they become available.

APPENDIX A. OPTICAL CONSTANTS FOR ITO AND FUSED QUARTZ

For completeness, we include refractive index information for the two antireflective coating materials considered in this paper. Text versions of the ITO dielectric constant parameters and the quartz index parameters may be found at `http://pdg.lbl.gov/~deg/ccd.html`, under "Data."

A.1. Tin-doped indium oxide (ITO)

Our main sources of information about the optical constants for indium-tin oxide are the papers by Gerfin & Grätzel[22] and Woollam, McGahan, & Johs.[23] Ref. 22 gives tables of 6-parameter fits to a dispersion formula for the dielectric constant ϵ. Figure 9(a) shows the index, calculated as the real part of $\sqrt{\epsilon}$, for three ITO films obtained from different sources. The fits based on data for $\lambda < 690$ nm. Data from a figure in Ref. 23 are shown by the irregular dotted line. We have used the functional form of Gerfin & Grätzel to draw the solid curve, which we use for our calculations. The curvature change and decrease of the index above 700 nm is expected from a Drude-type absorption edge, indicating free carriers in the film.

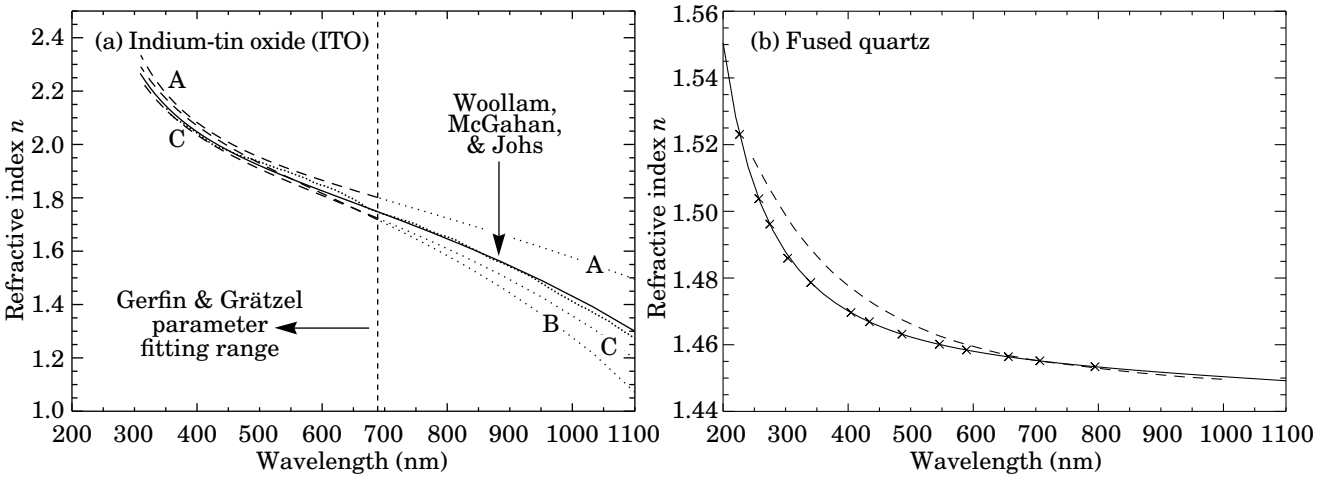

Figure 9. (a) Refractive index for tin-doped indium oxide (ITO) as obtained using the phenomenological fits by Gerfin & Grätzel[22] to spectroscopic ellipsometry data in the range 1.8 and 3.5 eV ($\lambda\lambda$ = 689–354 nm). Curves A, B, and C are for three different samples. The solid curve is a function of the same form drawn through the measurements of Woollam *et al.*[23] (irregular dotted curve). (b) The index of refraction for fused quartz, calculated from Eq. (15).[24] The $\times$'s indicate experimental measurements taken from Jenkins & White.[25] The dashed curve, also from Woollam *et al.*, is for a sputtered SiO_2 film.

Note that the ITO index falls below that of fused quartz in the near infrared. This limits the effectiveness of the ITO-quartz combination as an AR coating; in the future, films of other materials will be added.

Over the optical region the index is essentially real, and absorption can be neglected, particularly for the thin films we use here. Beyond the absorption edge ITO is conductive, and so in the LBNL application the film doubles as a back electrode to which the depletion voltage is applied.

A.2. Fused quartz

A fit to the measured index of fused quartz at 20° C, inspired by a three-pole dispersion formula, is given by Malitson[24] and reported in the Melles Griot catalog:

$$n^2 = 1 + \frac{0.6961663\,\lambda^2}{\lambda^2 - 0.0684043^2} + \frac{0.4079426\,\lambda^2}{\lambda^2 - 0.1162414^2} + \frac{0.8974794\,\lambda^2}{\lambda^2 - 9.896161^2} \tag{15}$$

(WARNING: Here λ is in μm.) The formula is claimed to be accurate to $\pm 3\times 10^{-5}$, and it is valid over the entire region of interest. This index is shown in Figure 9(b), along with experimental points obtained from Jenkins & White.[25]

There is some question as to whether a sputtered SiO_2 film has the same optical properties as fused quartz. Woollam *et al.*'s data for such a film are shown by the dashed line in the figure. The largest difference, about 0.01 at $\lambda \approx 350$ nm, is probably not important for our purposes even if real, especially given the uncertainties of the ITO index.

ACKNOWLEDGMENTS

We are grateful to our former collaborator Nadine Wang for ITO development work in the LBNL MicroSystems Lab, and to Susana Deustua for a critical reading of this manuscript. This work was supported by the U.S. Department of Energy under contract No. DE-AC03-76SF00098.

REFERENCES

1. D. F. Edwards, "Silicon (Si)," in *Handbook of Optical Constants of Solids*, E. D. Palik, ed., pp. 547–569, Academic Press, 1985.
2. J. R. Janesick, "Advanced applications of scientific charge coupled devices," *IS&T/SPIE Symposium on Electronic Imaging Science and Technology* , p. 233, (no data source or year given).
3. K. Rajkanan, R. Singh, and J. Shewchun, "Absorption coefficient of silicon for solar cell calculations," *Solid-State Electronics* **22**, pp. 793–795, 1979.
4. J. B. Oke *et al.*, "The Keck low-resolution imaging spectrometer," *Pub. Astron. Soc. Pac.* **107**, pp. 375–385, 1995.
5. G. E. Jellison, Jr. and F. A. Modine, "Optical constants for silicon at 300 and 10 K determined from 1.64 to 4.73 eV ellipsometry," *J. Appl. Phys.* **53**, pp. 3745–3753, 1982.
6. M. M. Blouke, W. A. Delamere, and G. Womack, "A simplified model of the back surface of a charge-coupled device," *SPIE* **1447**, pp. 142–155, 1991.
7. C. M. Huang, B. B. Kosicki, J. R. Theriault, J. A. Gregory, B. E. Burke, B. W. Johnson, and E. T. Hurley, "Quantum efficiency model for a p^+-doped back-illuminated CCD imager," *SPIE* **1447**, pp. 156–164, 1991.
8. S. E. Holland, G. Goldhaber, D. E. Groom, W. W. Moses, C. R. Pennypacker, S. Perlmutter, N. W. Wang, R. J. Stover, and M. Wei, "A 200×200 CCD image sensor fabricated on high-resistivity silicon," *IEDM Tech. Digest* , pp. 911–914, 1996.
9. S. Holland, G. Goldhaber, D. E. Groom, W. W. Moses, C. R. Pennypacker, S. Perlmutter, N. W. Wang, R. J. Stover, and M. Wei, "Development of back-illuminated, fully-depleted CCD image sensors for use in astronomy and astrophysics," *Proc. 1997 IEEE Workshop on Charge-Coupled-Devices and Advanced Image Sensors* , Bruges, Belgium, June 5-7, 1997.
10. J. R. Janesick and D. Campbell in *IEDM Tech. Digest*, p. 350, 1986.
11. G. Lubberts, B. C. Burkey, F. Moser, and E. A. Trabka, "Optical properties of phosphorus-doped polycrystalline silicon layers," *J. Appl. Phys.* **52**, pp. 6870–6878, 1981.
12. D. E. Aspnes and J. B. Theeten *J. Electrochem. Soc.* **127**, p. 1359, 1980; D. E. Aspnes and J. B. Theeten, private communication to D. F. Edwards (1980).
13. J. I. Pankove, "Optical processes in semiconductors," Chapter 3, Dover Publications, New York, 1975.
14. R. Braunstein, A. R. Moore, and F. Herman, "Intrinsic optical absorption in germanium-silicon alloys," *Phys. Rev.* **109**, pp. 695–710, 1958.
15. G. G. Macfarlane, T. P. McLean, J. E. Quarrington, and V. Roberts, "Fine structure in the absorption-edge spectrum of Si," *Phys. Rev.* **111**, pp. 1245–1254, 1958.
16. F. L. Pedrotti and L. S. Pedrotti, *Introduction to Optics*, Prentice Hall, New Jersey, 1993.
17. G. Stokes, *Mathematical and Physical Papers*, Vol. 2, pp. 89*ff*, especially p. 91.
18. R. J. Stover, M. Wei, D. K. Gilmore, S. E. Holland, D. E. Groom, W. W. Moses, S. Perlmutter, G. Goldhaber, C. R. Pennypacker, N. W. Wang, and N. Palaio, "Characterization of a fully depleted CCD on high-resistivity silicon," *SPIE* **3019**, pp. 183–188, 1997.
19. R. J. Stover, M. Wei, D. K. Gilmore, S. E. Holland, D. E. Groom, W. W. Moses, S. Perlmutter, G. Goldhaber, C. R. Pennypacker, N. W. Wang, and N. Palaio, "A high performance CCD on high resistivity silicon," *SPIE* **3505**, pp. 13–18, 1998.
20. M. M. Blouke and M. Nelson *SPIE* **1900**, pp. 228–240, 1993.
21. P. Jonsson, S. Faber, and A. Phillips, "Defringing," UCO/Lick Observatory (preliminary draft), 1998.
22. T. Gerfin and M. Grätzel, "Optical properties of tin-doped indium oxide determined by spectroscopic ellipsometry," *J. Appl. Phys.* **79**, p. 1722, 1996.
23. J. A. Woollam, W. A. McGahan, and B. Johs, "Spectroscopic ellipsometry studies of indium tin oxide and other flat panel display multilayer materials," *Thin Solid Films* **241**, pp. 44–46, 1994.
24. J. H. Malitson, "Interspecimen comparison of the refractive index of fused silica," *J. Opt. Soc. Am.* **55**, pp. 1205–1209, 1965, as reported in the Melles Griot Catalog.
25. F. A. Jenkins and H. E. White, *Fundamentals of Optics (2nd edition)*, p. 514, McGraw Hill, New York, 1950.